Dynamic driving eliminates volume fraction inhomogeneity and apparent yield stress in flowing dense non-Brownian suspensions ⊞

Christopher Ness ✉ ⓘ ; Amgad S. Moussa

Check for updates

View Online

Export Citation

Physics of Fluids

Special Topic:
Recent Advances in Fluid Dynamics and its Applications

Guest Editors: B.Reddappa, B. Rushi Kumar, Sreedhara Rao Gunakala, Bijula Prabhakar Reddy

Submit Today!

AIP Publishing

AIP Publishing

Dynamic driving eliminates volume fraction inhomogeneity and apparent yield stress in flowing dense non-Brownian suspensions EP

View Online   Export Citation   CrossMark

Christopher Ness[1,a)] iD and Amgad S. Moussa[2]

AFFILIATIONS

[1]School of Engineering, University of Edinburgh, Edinburgh EH9 3JL, United Kingdom
[2]Syngenta Crop Protection AG, 4058 Basel, Switzerland

[a)]Author to whom correspondence should be addressed: Chris.Ness@ed.ac.uk

ABSTRACT

Dense suspensions of non-Brownian hard spheres are often characterized as yield-stress fluids despite having no intrinsic time or force scales that could lead to such rheology. One mechanism for the apparent yield stress is particle migration, which produces (or is caused by) inhomogeneous flow conditions and leads to local regions where the solids' content approaches or exceeds the limit of flowability. In such a scenario, one does not induce flow by exceeding a yield stress, but instead by exploring the only remaining control parameter, namely the flow history. We demonstrate using particle-based simulation that this apparent local yield stress behavior does indeed emerge in a model dense suspension of non-Brownian hard spheres and that it can be eliminated by imposing a time-varying flow field.

I. INTRODUCTION

Dense suspensions of micrometer-sized particles are commonplace in industry, where effective modeling for design and operation of processes requires accurate and reliable material characterization.[1,2] In a model system of non-Brownian, non-inertial hard particles (relevant to systems with particle radius $a \approx 1$–$10 \, \mu$m) under steady homogeneous flow, the components of the stress tensor are linear in the shear rate and are functions of the particle volume fraction ϕ only.[3,4] For the shear viscosity, one can therefore write $\Sigma_{xy}/\eta\dot{\gamma} = \mathcal{F}(\phi)$, with η being the viscosity of the suspending liquid, Σ_{xy} the shear stress, and $\dot{\gamma}$ the shear rate. The function $\mathcal{F}$ is typically written in a general form as $\kappa(\phi_m - \phi)^{-\lambda}$[5,6] ($\lambda \approx 2$), with the maximum packing fraction ϕ_m being the key parameter needed to describe the rheology. Importantly, this frictional jamming point can be exceeded in some circumstances, since it is lower than the random close packing limit $\phi_{\mathrm{rcp}} \approx 0.64$.

Practitioners typically seek to characterize suspension rheology under well-controlled conditions and use the extracted parameters to make predictions for more complex engineering flow scenarios. In practice, this involves measuring, e.g., Σ_{xy} vs $\dot{\gamma}$ or $\Sigma_{xy}/\dot{\gamma}$ vs Σ_{xy} under conditions in which ϕ is presumed to be spatially invariant. Experiments with granular particles indeed found no yield stress below the frictional jamming point for the density-matched case in which the

particle distribution remains spatially uniform.[3,7] In cases where the stress field predisposes the system to particle migration, however, this approach can prove problematic. For a non-Brownian suspension in a Couette flow, for instance, one often finds an inner sheared region and an outer annulus that is non-flowing[8,9] (or much slower flowing[10,11]) and similarly a yield stress is reported in granular suspensions for which gravity causes settling.[7] This observation means that one could characterize the bulk constitutive behavior of the material using a model with a finite yield stress (see the discussion in Ref. 9) despite a simple dimensional analysis (mentioned earlier, see Boyer *et al.*[3]) demonstrating that this is not possible below ϕ_m. The non-flowing region appears due to the spatially varying ϕ that emerges as a result of normal stress gradients, so that the Herschel–Bulkley parameters obtained from such a measurement do not describe a flow curve *per se* but rather a series of points from a family of flow curves each with different ϕ. What is being measured is thus not a *local flow rule*[12,13] or constitutive behavior for a constant-ϕ material; consequently, the parameters measured under one set of flow conditions will inevitably fail to predict the flow behavior in others. More fundamentally, the non-flowing region is not indicative of a yield stress in a homogeneous material but rather of a spatial region in which the local ϕ approaches or even exceeds the jamming value ϕ_m.

22 August 2024 18:14:34

This subtle but important distinction has consequences for how one might achieve *unjamming* in practical scenarios, which we address here. In general, one achieves flow in a yield stress fluid by overcoming that stress. In non-Brownian suspensions in which particle migration is present, increasing the applied stress will fail to unjam the system (unless the particles are deformable). This must instead be achieved by changing the details of the flow protocol, a requirement deriving from the fragility of such materials and the tendency for their viscosity to decrease upon changes to flow direction.[14–16] Understanding this distinction in governing physics is crucial to achieving flow in jammed scenarios and has been explored in various contexts including vibration-induced liquefaction[17,18] and in more controlled superposed orthogonal shear.[19]

Here, we explore this problem using a computational thought experiment: a particle-based simulation modeling the Newtonian dynamics of suspended hard spheres under various imposed inhomogeneous flow conditions, accounting for pairwise hydrodynamic lubrication and frictional particle–particle contact forces.[20] Our imposed flow is a time-varying extension of that described by Saitoh and Tighe[21] (see also Refs. 22 and 23, although we address transient flows, which these works do not) and sets up volume fraction profiles that locally exceed ϕ_m, allowing us to demonstrate and then scrutinize the apparent yield stress behavior, before exploring under what conditions it can be eliminated.

II. NUMERICAL MODEL

We model a non-Brownian suspension of micrometer-sized spheres under an imposed driving force that leads to a spatially and temporally varying shear rate $\dot{\gamma}(y, t)$. The particle properties that set the length, mass, and time scales are the radius a (length), density ρ (mass/length^3) (equal to the fluid density), and stiffness k_n (mass/time^2) (this has a tangential counterpart $k_t = 0.7k_n$). Also relevant are the fluid viscosity η (mass/(length $\times$ time)), the solid volume fraction ϕ (dimensionless), and the interparticle friction coefficient $\mu = 0.5$ (dimensionless). The timescales $\sqrt{\rho a^3/k_n}$ and $\rho a^2/\eta$ are set $\ll 1/\dot{\gamma}$ so that the system meets the criteria for being rate-independent, and we set $(\rho a^2 h_{\min}/\eta)/\sqrt{\rho a^3/k_n} = 0.1$ so that contacts are fully overdamped ($h_{\min}$ is defined herein). At a steady state and with spatially uniform $\dot{\gamma}$, the dimensionless shear stress $\Sigma_{xy}/\eta\dot{\gamma}$ is thus a function of ϕ only.[3]

Particles are subject to Stokes drag, pairwise lubrication, and pairwise contact forces and torques.[24] The drag on particle i (radius a_i) is set by its velocity $\boldsymbol{u}_i$ and the specified fluid streaming velocity at its center $\boldsymbol{u}^\infty(\boldsymbol{x}_i)$: $\boldsymbol{F}_i^d = -6\pi\eta a_i(\boldsymbol{u}_i - \boldsymbol{u}^\infty(\boldsymbol{x}_i))$. Similarly, a torque acts to cause the particles to rotate with angular velocity set by $\frac{1}{2}(\nabla \times \boldsymbol{u}^\infty)$. Neighboring particles i and j with center-to-center vector $\boldsymbol{r}_{i,j}$ experience lubrication forces[25,26] dependent on the dimensionless gap h between their surfaces and their relative velocity. The leading term scales with $1/h$ and the normal component (along $\boldsymbol{r}_{i,j}$) of the pairwise velocity difference: $\boldsymbol{F}_{i,j}^l = \frac{3}{2}\pi a_i\eta\frac{1}{h}(\boldsymbol{u}_j - \boldsymbol{u}_i)_n$. Lubrication forces oppose relative motion between particles and are prevented from diverging at contact by an imposed lower limit on h, $h_{\min} = 10^{-3}$ (with results insensitive to this choice when $10^{-4} < h_{\min} < 10^{-2}$). A torque also acts to resist relative rotation between i and j, detailed elsewhere.[20] Contacting particles i and j experience repulsive forces dependent on the scalar overlap $\delta = 2a - |\boldsymbol{r}_i - \boldsymbol{r}_j|$ and the absolute

tangential displacement accumulated over the duration of the contact ξ: $\boldsymbol{F}_{i,j}^c = k_n\delta\boldsymbol{r}_{i,j}/|\boldsymbol{r}_{i,j}| - k_t\xi$. The friction coefficient μ sets an upper bound on ξ through $|\xi| \leq \mu k_n\delta/k_t$. The α, β component of the stress Σ due to lubrication and contact is found, respectively, by summing $(F_{i,j}^{l,\alpha}r_{i,j}^\beta + F_{i,j}^{l,\beta}r_{i,j}^\alpha)/2$ and $F_{i,j}^{c,\alpha}r_{i,j}^\beta$ over all pairs. The forces are summed on each particle, and the trajectories are then updated with time step chosen to be small compared to $\sqrt{\rho a^3/k_n}$ and $\rho a^2/\eta$.

III. STEADY STATE INHOMOGENEOUS FLOW

For inhomogeneous flow simulations, we set the periodic simulation box size as $L_x = 60a$ and $L_z = 20a$, with $L_y = 100a, 200a, 400a$ [Fig. 1(a)] so that there is scale separation between the domain size in the velocity gradient direction and the particle, and we initialize the system with a spatially homogeneous volume fraction of $\bar{\phi} = 0.59$ (fractionally below the simple shear jamming point). Simulations comprise $\approx 40\,000$ particles with radii a and $1.4a$ mixed in equal numbers, chosen to prevent crystallization while retaining rheology and jamming points close to the idealized monodisperse limit.[27]

We drive flow by manipulating the per-particle Stokes drag term described earlier, applying a streaming velocity $\boldsymbol{u}^\infty$ as

$$\boldsymbol{F}_i^d = -6\pi\eta a_i\left(\boldsymbol{u}_i - \underbrace{\alpha_1\sin\left(\frac{2\pi y_i}{L}\right)\boldsymbol{\delta}_x}_{\boldsymbol{u}^\infty}\right). \quad (1)$$

Here, y_i is the y-coordinate of particle i, and $\boldsymbol{\delta}_x$ is a unit vector pointing along x. This $\boldsymbol{u}^\infty$ is sketched in Fig. 1(a). This force introduces a timescale $L/2\pi\alpha_1$, which compares against the viscous timescale to give a dimensionless control parameter $\rho(2\pi\alpha_1/L)a^2/\eta$. Setting this quantity $\mathcal{O}(10^{-2})$ results in local Stokes numbers $\rho\dot{\gamma}(y)a^2/\eta \leq 10^{-2}$ so that particle inertia can be neglected. In this range, shear rates and stresses scale linearly with α_1 (equivalent to the rate-independent result for simple shear[3]). We focus first on the steady-state behavior, before addressing the dynamics associated with startup and time-varying driving.

Shown in Figs. 1(b)–1(e) are steady state profiles in y of the normal Σ_{yy} and shear Σ_{xy} stresses rescaled by a characteristic stress $\eta(2\pi\alpha_1/L)$, the shear rate $\rho\dot{\gamma}a^2/\eta$, and the volume fraction ϕ. We first demonstrate that the rheology is in violation of a local flow rule, having obtained the latter using simple shear simulations with $\boldsymbol{F}_i^d = -6\pi\eta a_i(\boldsymbol{u}_i - \dot{\Gamma}y_i/L\boldsymbol{\delta}_x)$ for constant $\dot{\Gamma}$ and varying ϕ. Figure 1(f) shows the homogeneous shear and normal stresses, with solid lines showing fits to $\Sigma_{yy}/\eta\dot{\gamma} = \tilde{\kappa}(\phi_m - \phi)^{-2}$ and $\Sigma_{xy}/\eta\dot{\gamma} = \kappa(\phi_m - \phi)^{-2}$, with $\phi_m = 0.595$, $\tilde{\kappa} = 0.15$, and $\kappa = 0.09$. Using the measured, spatially uniform normal stresses from inhomogeneous flow [from Fig. 1(b)] and the imposed $\boldsymbol{u}^\infty$ [gray line Fig. 1(d)], we predict the profiles in y of volume fraction $\phi(y) = \phi_m - (\tilde{\kappa}\eta|\dot{\gamma}(y)|/\Sigma_{yy})^{1/2}$ and shear stress $\Sigma_{xy}(y) = \kappa\eta\dot{\gamma}(\phi_m - \phi(y))^{-2}$ [broad lines in Figs. 1(c) and 1(e)]. Despite being bound by ϕ_m as the maximum allowed value of ϕ and having to conform to the imposed shear rate, the local assumption makes reasonable predictions of $\phi(y)$ and $\Sigma_{xy}(y)$ in regions where $\rho\dot{\gamma}(y)a^2/\eta$ is large, but around $y/L = 0.25$ and 0.75, it fails dramatically. In particular, the measured ϕ is able to exceed significantly the homogeneous ϕ_m in large regions of the domain (although it remains bounded by the close-packing limit $\phi_{\text{rcp}} \approx 0.64$), confirming that the local flow rule measured under homogeneous conditions
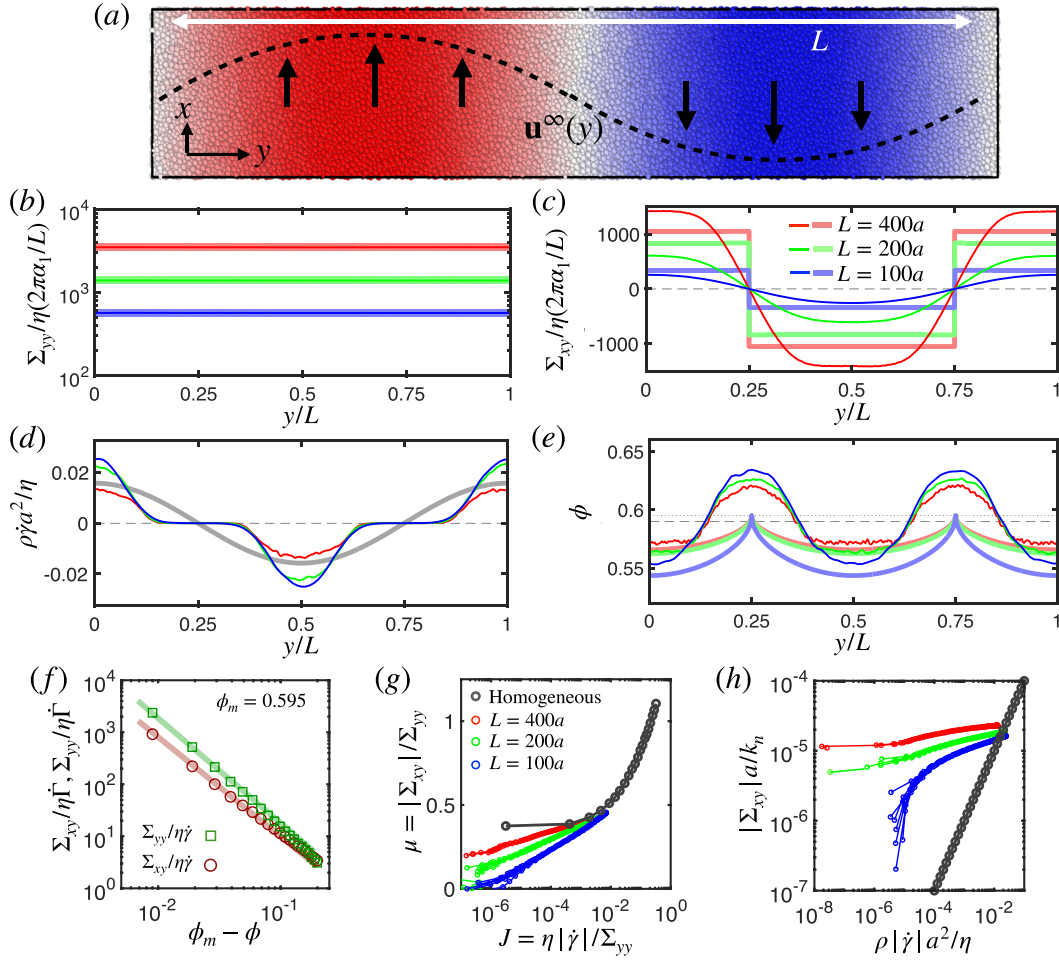
FIG. 1. Steady state inhomogeneous flow. (a) Snapshot of simulation. Dashed line indicates the magnitude of the streaming velocity applied to each particle according to its y position, with small arrows and color scale indicating the flow direction. Shown in (b)–(e) are profiles in y of, respectively, the normal stress $\Sigma_{yy}/\eta(2\pi\alpha_1/L)$; the shear stress $\Sigma_{xy}/\eta(2\pi\alpha_1/L)$; the dimensionless shear rate $\rho\dot{\gamma}a^2/\eta$; and the volume fraction ϕ [with the black dashed line in (e) indicating the mean $\bar{\phi} = 0.59$ and the dotted line indicating $\phi_m = 0.595$, with $L = 400a$ (red), $L = 200a$ (green), $L = 100a$ (blue)]. Broad colored lines in (b), (c), and (e) represent predictions of the local constitutive model described in the text, assuming the flow follows the imposed $\boldsymbol{u}^\infty$ [gray line in (d)]. (f) Local rheology measured with $\rho\dot{\gamma}a^2/\eta = 0.01$, showing the shear (red) and normal (green) stresses as functions of ϕ. Solid lines are fits to the local model described in the text. In (g) and (h) are rheology data presented parametrically as $\mu(y)$ vs $J(y)$ and $|\Sigma_{xy}(y)|a/k_n$ vs $\rho|\dot{\gamma}(y)|a^2\eta$. Gray points and lines indicate homogeneous data; colored lines represent inhomogeneous data with different L (colors as above), with each point representing a y position.

does not apply (measuring ϕ_m with greater precision would not change this conclusion). These regions have very low shear rate and are indicative of narrow plug-like regions. The spatial variation of ϕ emerges as a consequence of a transient gradient in the normal stress Σ_{yy} during start up.[10] In the steady state, once the ϕ profile has established, Σ_{yy} is uniform across y [Fig. 1(b)].

Representative flow curves obtained under steady state sinusoidal driving are shown parametrically in Figs. 1(g) and 1(h). Figure 1(g) shows the "$\mu(J)$"-rheology under inhomogeneous flow (colors), compared against simple shear (gray), where the latter corresponds well to canonical experiments.[3] Here, each colored point represents a binned region in y of width $\approx a$, with each plotted point thus representing a different volume fraction. Consistent with the y-profiles [Figs. 1(b)–1(e)], inhomogeneous data violate the simple shear

rheology when the shear rate is low, with $L = 100a$ data reaching $\mu = 0$ and data for larger system sizes consistently decreasing with shear rate over the range of accessible J. Figure 1(h) plots the local reduced shear stress $|\Sigma_{xy}|a/k_n$ vs the local shear rate $\rho\dot{\gamma}(y)a^2/\eta$, again with each plotted point representing a specific y-coordinate and thus having a different volume fraction. Each plotted point thus represents a single point taken from one of a family of volume fraction-dependent homogeneous constitutive curves, with an example given in gray for the global volume fraction of the system. For $L = 400a$, the inhomogeneous data clearly tend toward an apparent yield stress as $\dot{\gamma} \to 0$ (noting that $\Sigma_{xy} = 0$ precisely at the spatial position where $\dot{\gamma} = 0$), whereas this effect is weakened as the gradient of the driving flow is increased, suggesting that the importance of the apparent yield stress and its behavior under dynamic flow described below becomes more

important in larger geometries. [Indeed, most practical geometries in which dense suspensions arise will have shear rate gradients spanning lengthscales much larger than $\mathcal{O}(100a)$]. Importantly, the data in Fig. 1(h) is not a true flow curve: each data point is measured at a different y position, for which the local ϕ is varying according to Fig. 1(e). Rather, we plot a series of points each taken from a separate rate-independent flow curve. Nonetheless, what is important is that in this representation the viscosity diverges as the shear rate is lowered (equivalently $\Sigma_{xy} \to$ constant as $\dot{\gamma} \to 0$) and $\phi > \phi_m$, superficially representing yield stress behavior. This phenomenology occurs for $\bar{\phi} = 0.59$, where under homogeneous conditions, the material flows viscously (albeit with large viscosity).

IV. TRANSIENT FLOW

Following the reasoning that leads to rate-independence in steady states for non-Brownian suspensions, one finds that the stress may also depend on the flow history. This is well-supported by experimental data, notably the pioneering flow-reversal experiments of Gadala-Maria and Acrivos,[28] and later demonstrations that time-varying flow can reduce the viscosity of shear thickening suspensions.[19] From this, we infer that time-varying flow fields can produce behavior that violates the steady state (homogeneous or inhomogeneous) rheology, a result that is well-established in spatially uniform flows.[19,29] A central question to the latter works is how fast does the flow need to vary in order to produce novelty.
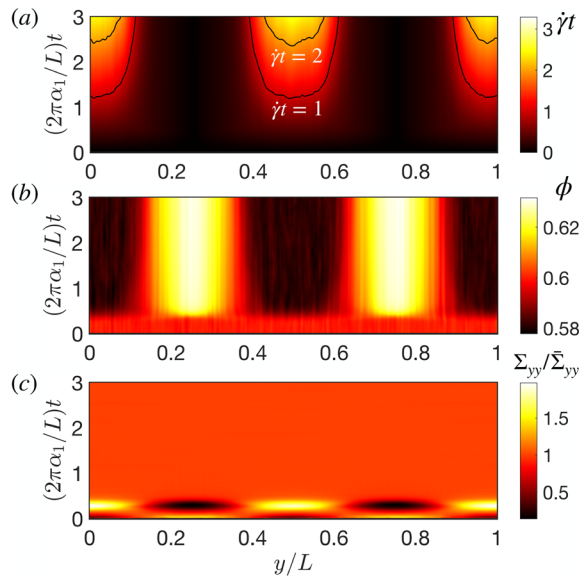
In the absence of other time or force scales (thermal motion, attractive or repulsive interactions), the only relevant timescale in our model is the time taken to establish the inhomogeneous volume fraction profile $\phi(y)$ shown in Fig. 1(e). Since we are operating under rate-independent conditions (i.e., since $\rho\dot{\gamma}a^2/\eta$ is small), it is more appropriate to consider the *strain* taken to establish the ϕ profile, since (in the linear regime) the time taken will scale inversely with the characteristic timescale for driving flow in our model, $L/2\pi\alpha_1$.

To determine to rate at which our system advances toward spatially inhomogeneous steady states, we consider startup flow during the transient period from $t = 0$ (when the particle distribution is uniform in space) up until the steady states in Fig. 1 are reached, Fig. 2. Starting from a homogeneous particle distribution [$\phi \neq \phi(y)$] with no shear [$\dot{\gamma}(y) = 0$], the system reaches an established $\phi(y)$ profile once the elapsed time is such that $(2\pi\alpha_1/L)t \approx 1$, corresponding to a strain of ≈ 1 along the sheared regions. Over the same duration, one observes the normal stress obtaining a spatially uniform value, indicating that beyond $\dot{\gamma}t = 1$ there is no driving force for further particle migration.

In order to disrupt particle migration and mitigate against regions with $\phi > \phi_m$, one must introduce a driving flow that changes its position more rapidly than the inhomogeneous volume fraction profile can establish. Defining a characteristic velocity scale for the time-varying driving as α_2 (see below), we might expect such dynamic driving to influence the steady state particle distribution when $\alpha_2/\alpha_1 \gtrsim 1$. This dimensionless ratio operates in some sense as a Peclet number, comparing the size of the fluctuations or perturbations to the system to the
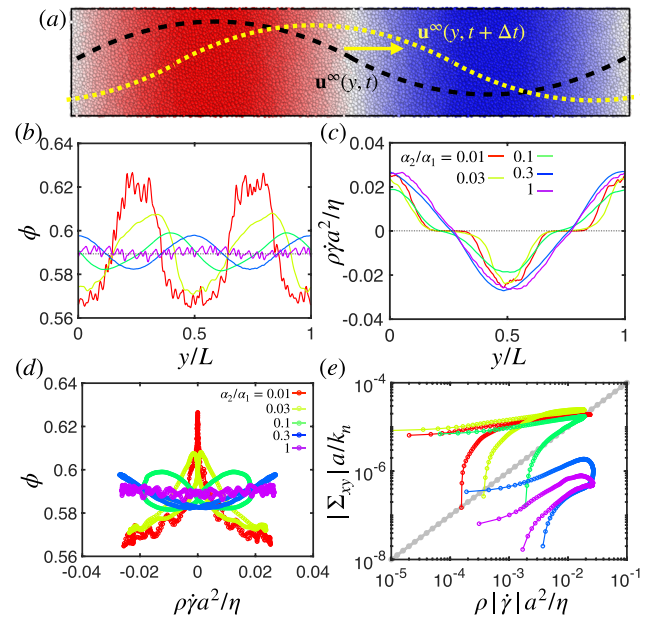

FIG. 2. Time series of the initial transient after starting up from a spatially uniform state. Horizontal axis represents the spatial position in y; vertical axis is increasing time t; color bar gives the accumulated strain (a) and volume fraction, (b) and normal stress, and (c) profiles. (a) Accumulated strain profile $|\dot{\gamma}(y)|t$, showing a steady increase in the strain along $y/L = 0, 0.5, 1$ and no accumulated strain in the regions at $y/L = 0.25, 0.75$ where $\dot{\gamma} \approx 0$. Solid black lines are contours at integer values of $\dot{\gamma}t$. (b) Development of volume fraction profile $\phi(y)$ with time. The time t on the vertical axis is scaled with the characteristic time associated with driving, $L/2\pi\alpha_1$. (c) Development of the uniform normal stress profile $\Sigma_{yy}(y)$ occurs within the initial 0.5 strain units, consistent with the evolution of the ϕ field. Here, Σ_{yy} is rescaled by its spatially averaged value at each time step $\bar{\Sigma}_{yy}$.

FIG. 3. Response to driving with a spatially and temporally varying $\boldsymbol{u}^\infty$. (a) Snapshot of the simulation showing the applied driving $\boldsymbol{u}^\infty(y)$ at time t in black and at some later time $t + \Delta t$ in yellow, (b) volume fraction profiles $\phi(y)$ for varying α_2/α_1 [see legend in (c)], (c) shear rate profiles $\rho\dot{\gamma}a^2/\eta$ for varying α_2/α_1, (d) phase shift in ϕ, $\dot{\gamma}$ for varying α_2/α_1, and (e) apparent flow curves obtained by parametric plots of $|\Sigma_{xy}(y)|a/k_n$ vs $\rho|\dot{\gamma}(y)|a^2\eta$ for varying α_2/α_1, with gray line indicating homogeneous result.

translation driven by the mean flow. Works that applied vibrations to granular packings in other settings similarly found that increasing the magnitude of imposed noise (analogous but not identical to our moving flow field) resulted in liquefaction of the material.[17,30]

V. DYNAMIC INHOMOGENEOUS FLOW

To test this idea, we apply a time-varying driving force, given by a modified version of the drag used earlier,

$$\boldsymbol{F}_i^d = -6\pi\eta a_i\left(\boldsymbol{u}_i - \alpha_1 \sin\left(\frac{2\pi}{L}(y_i + \alpha_2 t)\right)\boldsymbol{\delta}_x\right). \qquad (2)$$

This form [sketched in Fig. 3(a)] is chosen as the most simple way to introduce time-dependence into the model beyond the initial transient. It produces a sinusoidal form for $\boldsymbol{u}^\infty$ that translates in the $+y$ direction with constant velocity set by α_2. The nature of the flow is then given by a competition between the downstream flow driving determined by α_1, and the rate of change of the flow direction determined by α_2. Importantly, it is not sufficient to simply vary α_1 in time with $\alpha_2 = 0$. The resulting "pulsed" flow would, under rate-independent conditions, not lead to a change in the net path followed by particles (it would only change the rate at which their path is followed) and so would not change the bulk rheology in Figs. 1(g) and 1(h).

Shown in Figs. 3(b)–3(e) are steady state results for $\alpha_2/\alpha_1 = [0, 1]$, where the horizontal axes in (b) and (c) are shifted so that $y/L = 0$ maps to $\boldsymbol{F}_i^d = 0$. In each case, we initialized the system with $\alpha_2 = 0$ so that ϕ locally exceeded ϕ_m. Focusing on the volume fraction profile $\phi(y)$, Fig. 3(b), we see that increasing α_2/α_1 leads to a homogenization of the system, i.e., $\phi(y)$ becoming spatially uniform. This is associated with the shear rate profile more closely following the imposed affine flow, Fig. 3(c). For $\alpha_2/\alpha_1 = 0.1$, $\phi(y)$ becomes distorted with the peaks being lowered and shifted. The phase shift in the ϕ peaks is explainable in terms of a momentum balance per unit volume in y taken from a reference point moving at α_2. For $\alpha_2 = 0$, one obtains steady states when the $\dot{\gamma}$ and ϕ profiles are such that $\frac{\partial}{\partial y}\Sigma_{yy} = 0$ (though the non-local constitutive relation governing this balance is elusive). Here, the symmetry is such that positions in space separated by $y/L = 0.25$ are equivalent up to a factor ± 1. For $\alpha_2 \neq 0$, $\frac{\partial}{\partial y}\Sigma_{yy}$ at each y position must balance the change in momentum associated with a flux through that position with rate α_2 but time-varying ϕ. This leads to ϕ and $\dot{\gamma}$ becoming out of phase, Fig. 3(d), so that the symmetry is broken and instead positions separated by $y/L = 0.5$ are equivalent. At $\alpha_2/\alpha_1 = 1$, the system is completely homogeneous in terms of the particle distribution in y.

This change in the arrangement of particles is reflected in the measured rheology. Plotting the stress against strain rate, Fig. 3(e), we see a progressive shift from the apparent yield stress behavior to a more rate-dependent response when $\alpha_2/\alpha_1 = 1$. In the latter case, the two branches of the flow curve (in pink) show the stress increasing with shear rate (both being approximately linear over a narrow range), with the stress at all shear rates being lower than the simple shear one obtained at the same global volume fraction (shown in light gray). The rheology here is bivalued since the breaking of symmetry described earlier leads to states of distinct ϕ (separated by $y/L = 0.25$), sharing a common $|\dot{\gamma}|$. Here, the rapidly changing driving flow acts similarly to the vibrations described by Ref. 17 and the orthogonal shear described by Ref. 19, that is, perturbing the instantaneous shear rate sufficiently

fast that a steady microstructure cannot be established. Thus, by changing the flow field rapidly, we demonstrate and utilize the flow-history dependence of the material, noting that the relevant competition of timescales does not involve an internal material relaxation time (as would be the case in a thixotropic material) but rather the ratio of the driving timescales represented by α. In the inhomogeneous flow presented here, the comparatively rapid perturbation at large α has the additional effect of homogenizing the volume fraction profile. Recognizing that the response time to changes of flow direction decreases with increasing proximity to jamming,[31] it is likely that the value of α needed to eliminate the apparent yield stress will increase with the global volume fraction of the system, although this dependence is likely to be complex and warrants further investigation. Similarly, other factors that influence the position of the jamming point of the system such as polydispersity[27] and particle shape[32] will be important in governing the responsiveness of the material to dynamic inhomogeneous driving.

VI. CONCLUDING REMARKS

We have shown that inhomogeneous flow in dense non-Brownian suspensions drives particle migration, leading to a spatially varying volume fraction that can locally exceed the simple shear frictional jamming point ϕ_m by a significant amount. This effect can be eliminated by imposing a time-varying flow, choosing the timescale for the variation to be shorter than the characteristic time required for the spatial ϕ profile to establish. Importantly, achieving elimination of the apparent yield stress does not require us to exceed any critical stress (indeed, we can make our flow rates arbitrarily small by manipulating the parameter α_1, providing its ratio to α_2 is set appropriately). This illustrates important issues related to the flow physics of non-Brownian hard sphere suspensions: while the steady state homogeneous rheology is becoming well-characterized and well-understood (including links to rate-dependent phenomena such as shear thickening), inhomogeneous flow, and in particular, time-dependent inhomogeneous flows pose a major challenge to modeling and flow prediction.[22] This has direct consequences for industrial practice where knowing the relevant scale of the parameter α might guide the design of baffles or impellers in stirred tanks[33] or milling processes (for which particle-based simulation is increasingly providing mechanistic insight[34,35]) and may have far-reaching implications for fields as diverse as understanding translocation in biological systems.[36]

AUTHOR DECLARATIONS
Conflict of Interest

The authors have no conflicts to disclose.

Author Contributions

Christopher Ness: Conceptualization (equal); Data curation (equal); Formal analysis (equal); Investigation (equal); Methodology (equal); Writing – original draft (equal); Writing – review & editing (equal). **Amgad S. Moussa:** Conceptualization (equal); Methodology

22 August 2024 18:14:34

(equal); Writing – original draft (equal); Writing – review & editing (equal).

DATA AVAILABILITY

The data that support the findings of this study are available from the corresponding author upon reasonable request.

REFERENCES

[1] C. Ness, R. Seto, and R. Mari, "The physics of dense suspensions," Annu. Rev. Condens. Matter Phys. **13**, 97 (2022).

[2] J. J. Stickel and R. L. Powell, "Fluid mechanics and rheology of dense suspensions," Annu. Rev. Fluid Mech. **37**, 129 (2005).

[3] F. Boyer, É. Guazzelli, and O. Pouliquen, "Unifying suspension and granular rheology," Phys. Rev. Lett. **107**, 188301 (2011).

[4] É. Guazzelli and O. Pouliquen, "Rheology of dense granular suspensions," J. Fluid Mech. **852**, P1 (2018).

[5] I. M. Krieger and T. J. Dougherty, "A mechanism for non-Newtonian flow in suspensions of rigid spheres," Trans. Soc. Rheol. **3**, 137 (1959).

[6] S. Mueller, E. Llewellin, and H. Mader, "The rheology of suspensions of solid particles," Proc. R. Soc. A **466**, 1201 (2010).

[7] A. Fall, F. Bertrand, G. Ovarlez, and D. Bonn, "Yield stress and shear banding in granular suspensions," Phys. Rev. Lett. **103**, 178301 (2009).

[8] D. Leighton and A. Acrivos, "The shear-induced migration of particles in concentrated suspensions," J. Fluid Mech. **181**, 415 (1987).

[9] G. Ovarlez, F. Bertrand, and S. Rodts, "Local determination of the constitutive law of a dense suspension of noncolloidal particles through magnetic resonance imaging," J. Rheol. **50**, 259 (2006).

[10] J. F. Morris and F. Boulay, "Curvilinear flows of noncolloidal suspensions: The role of normal stresses," J. Rheol. **43**, 1213 (1999).

[11] R. J. Phillips, R. C. Armstrong, R. A. Brown, A. L. Graham, and J. R. Abbott, "A constitutive equation for concentrated suspensions that accounts for shear-induced particle migration," Phys. Fluids A **4**, 30 (1992).

[12] K. Kamrin and G. Koval, "Nonlocal constitutive relation for steady granular flow," Phys. Rev. Lett. **108**, 178301 (2012).

[13] M. Bouzid, M. Trulsson, P. Claudin, E. Clément, and B. Andreotti, "Nonlocal rheology of granular flows across yield conditions," Phys. Rev. Lett. **111**, 238301 (2013).

[14] M. Cates, J. Wittmer, J.-P. Bouchaud, and P. Claudin, "Jamming, force chains, and fragile matter," Phys. Rev. Lett. **81**, 1841 (1998).

[15] F. Peters, G. Ghigliotti, S. Gallier, F. Blanc, E. Lemaire, and L. Lobry, "Rheology of non-Brownian suspensions of rough frictional particles under shear reversal: A numerical study," J. Rheol. **60**, 715 (2016).

[16] V. G. Kolli, E. J. Pollauf, and F. Gadala-Maria, "Transient normal stress response in a concentrated suspension of spherical particles," J. Rheol. **46**, 321 (2002).

[17] C. Hanotin, S. K. De Richter, P. Marchal, L. J. Michot, and C. Baravian, "Vibration-induced liquefaction of granular suspensions," Phys. Rev. Lett. **108**, 198301 (2012).

[18] P. Sehgal, M. Ramaswamy, I. Cohen, and B. J. Kirby, "Using acoustic perturbations to dynamically tune shear thickening in colloidal suspensions," Phys. Rev. Lett. **123**, 128001 (2019).

[19] N. Y. C. Lin, C. Ness, M. E. Cates, J. Sun, and I. Cohen, "Tunable shear thickening in suspensions," Proc. Nat. Acad. Sci. **113**, 10774 (2016).

[20] O. Cheal and C. Ness, "Rheology of dense granular suspensions under extensional flow," J. Rheol. **62**, 501 (2018).

[21] K. Saitoh and B. P. Tighe, "Nonlocal effects in inhomogeneous flows of soft athermal disks," Phys. Rev. Lett. **122**, 188001 (2019).

[22] J. J. J. Gillissen and C. Ness, "Modeling the microstructure and stress in dense suspensions under inhomogeneous flow," Phys. Rev. Lett. **125**, 184503 (2020).

[23] B. P. Bhowmik and C. Ness, "Scaling description of frictionless dense suspensions under inhomogeneous flow," Phys. Rev. Lett. **132**, 118203 (2024).

[24] C. Ness, "Simulating dense, rate-independent suspension rheology using LAMMPS," Comput. Part. Mech. **10**, 2031 (2023).

[25] S. Kim and S. J. Karrila, *Microhydrodynamics: Principles and Selected Applications* (Butterworth Heinemann, 1991).

[26] D. Jeffrey, "The calculation of the low Reynolds number resistance functions for two unequal spheres," Phys. Fluids A **4**, 16 (1992).

[27] R. S. Farr and R. D. Groot, "Close packing density of polydisperse hard spheres," J. Chem. Phys. **131**, 244104 (2009).

[28] F. Gadala-Maria and A. Acrivos, "Shear-induced structure in a concentrated suspension of solid spheres," J. Rheol. **24**, 799 (1980).

[29] R. Niu, M. Ramaswamy, C. Ness, A. Shetty, and I. Cohen, "Tunable solidification of cornstarch under impact: How to make someone walking on cornstarch sink," Sci. Adv. **6**, eaay6661 (2020).

[30] C. Garat, S. Kiesgen de Richter, P. Lidon, A. Colin, and G. Ovarlez, "Using good vibrations: Melting and controlled shear jamming of dense granular suspensions," J. Rheol. **66**, 237 (2022).

[31] C. Ness and J. Sun, "Two-scale evolution during shear reversal in dense suspensions," Phys. Rev. E **93**, 012604 (2016).

[32] N. M. James, H. Xue, M. Goyal, and H. M. Jaeger, "Controlling shear jamming in dense suspensions via the particle aspect ratio," Soft Matter **15**, 3649 (2019).

[33] H. Yoon, D. Hill, S. Balachandar, R. Adrian, and M. Ha, "Reynolds number scaling of flow in a Rushton turbine stirred tank. Part I—Mean flow, circular jet and tip vortex scaling," Chem. Eng. Sci. **60**, 3169 (2005).

[34] R. Cabiscol, T. Jansen, M. Marigo, and C. Ness, "Application of hydrodynamic lubrication in discrete element method (DEM) simulations of wet bead milling chambers," Powder Technol. **384**, 542 (2021).

[35] Y. S. Tanneru, J. H. Finke, C. Schilde, Y. M. Harshe, and A. Kwade, "Coupled CFD-DEM simulation of pin-type wet stirred media mills using immersed boundary approach and hydrodynamic lubrication force," Powder Technol. **444**, 120060 (2024).

[36] A. Hosoi and D. I. Goldman, "Beneath our feet: Strategies for locomotion in granular media," Annu. Rev. Fluid Mech. **47**, 431 (2015).